LANGMUIR Article
Cite This: Langmuir 2019, 35, 4397−4402
pubs.acs.org/Langmuir

# Capillary Stress and Structural Relaxation in Moist Granular Materials

Tingtao Zhou,[†] Katerina Ioannidou,[‡,⊥] Enrico Masoero,[§] Mohammad Mirzadeh,[∥] Roland J.-M. Pellenq,[*,‡,⊥] and Martin Z. Bazant[*,∥,#]

[†]Department of Physics, [‡]MultiScale Materials Science for Energy and Environment (MSE2), The Joint CNRS-MIT-Aix-Marseille University Laboratory, UMI CNRS 3466, [∥]Department of Chemical Engineering, [⊥]Department of Civil and Environmental Engineering, and [#]Department of Mathematics, Massachusetts Institute of Technology, Cambridge, Massachusetts 02139, United States

[§]School of Engineering, Newcastle University, Newcastle upon Tyne NE1 7RU, U.K.

Supporting Information

**ABSTRACT:** A numerical and theoretical framework to address the poromechanical effect of capillary stress in complex mesoporous materials is proposed and exemplified for water sorption in cement. We first predict the capillary condensation/evaporation isotherm using lattice-gas simulations in a realistic nanogranular cement model. A phase-field model to calculate moisture-induced capillary stress is then introduced and applied to cement at different water contents. We show that capillary stress is an effective mechanism for eigenstress relaxation in granular heterogeneous porous media, which contributes to the durability of cement.

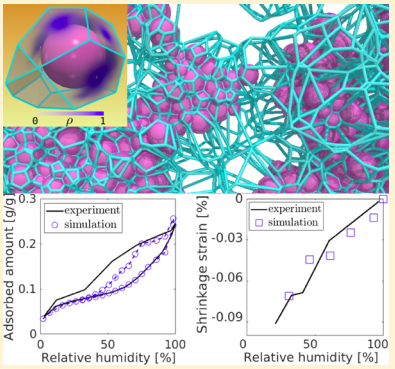


## INTRODUCTION

Capillary condensation is a ubiquitous process of vapor−liquid phase transition in porous media, such as sand piles, plaster, paints, silica gels, and cementitious materials, which has an important yet poorly understood effect on mechanical behavior. The confined fluid can generate enormous local stresses, as observed in granular material aging,[1] wet floor friction,[2] nanotribology,[3] multiphase immiscible flows,[4,5] cement drying shrinkage,[6,7] and in everyday life experiences such as hardening of a drying sponge or building a sand castle on the beach.[8] Capillary condensation and evaporation potentially bring undesirable fracture processes, as in drying and cracking of colloidal films[9,10] and paints,[11] but capillary stress can also can be exploited in nanomaterial fabrication by capillary force lithography,[12] capillary rise infiltration,[13,14] evaporation-driven assembly and self-organization,[15−18] and composite imbibition[19] and even used to evaluate the atmosphere of planets.[20]

Despite the broad importance of capillary forces, they remain challenging to predict in complex porous materials over the full range of liquid saturation, either in equilibrium or during a dynamical process of drainage/imbibition. For granular or colloidal materials, existing models addressing partial saturations are oversimplified and only apply either to low humidity (the so called pendular/funicular regimes)[21−23] or to idealized geometries (slit/cylindrical independent pores or a single sphere against a wall).[24−27] At higher saturation, models based on geometrical analysis of the Young−Laplace equation for smaller clusters[28,29] are proposed but restricted to only equilibrium liquid distributions inside monodisperse packings. A full molecular treatment here is beyond the current computational capability because that will require considering hundreds of millions of water molecules for our system.

Structural changes due to adsorption/desorption in porous media are known as "sorption-induced deformation". We refer the reader to Gor et al.[30] for a review on the topic. We also refer the readers to the recent work of Schappert and Pelster[31] reporting the poromechanics of Vycor, a porous silica glass, upon argon sorption. In this work, an unexpected sharp contraction followed by re-expansion was observed upon desorption. Notice that here, we are concerned with capillary stress-induced deformation only, therefore surface effects (Bangham effect[32]) that might occur at low relative humidity are beyond the scope of this work.

In this article, we propose a numerical and theoretical framework to quantitatively predict capillary condensation/evaporation[33,34] and compute associated capillary forces and structural relaxation in a 3D realistic nanogranular cement paste model[35] using lattice-gas simulations of adsorbed water[36]

**Received:** October 9, 2018
**Revised:** January 11, 2019
**Published:** February 24, 2019






DOI: 10.1021/acs.langmuir.8b03400
Langmuir 2019, 35, 4397−4402

parametrized from atomistic simulations.[37] In particular, this allowed us to access the adsorption/desorption mechanism and assess the role of (metastable) cavitation.[38] In addition, we present for the first time to our knowledge, a phase-field model of the liquid−vapor mixture spatial distribution, whose inhomogeneous stress tensor is integrated over Voronoi polyhedra in order to calculate forces between each pair of neighboring grains. The capillary forces applied to the cement hydrate the nanograins in molecular dynamics (MD) simulations, and together with the cohesive interactions between these nanograins predict the overall stress relaxation. As an important application, we calculate drying shrinkage of cement paste,[6,39−41] where the heterogeneous and multiscale, fully connected porous network induces significant mechanical irreversibilities during the drying−wetting cycles,[42] disqualifying simple models based on macroscopic homogenized poromechanics concepts, hence ignoring local heterogeneities in the pore voids and solid−fluid interactions.

## METHODS

**Capillary Condensation/Evaporation Isotherm.** We simulated capillary condensation and evaporation processes in our previously developed realistic mesoscale model of cement paste,[35] using a discrete lattice gas density functional theory (DFT) with interaction parameters imported from water/cement atomistic simulations.[37] This DFT approach was first derived by Kierlik et al.[36,43] for adsorption/desorption of a fluid in a quenched random porous solid. This method has been further applied to Vycor,[44] controlled porous silica glasses and aerogels,[45,46] to infer qualitatively adsorption/desorption isotherms through the minimization of the grand potential

$$\Omega = -w_{ff}\sum_{\langle i,j\rangle}\rho_i\rho_j - w_{sf}\sum_{i,j}\rho_i\eta_j - \mu\sum_i\rho_i + k_BT\sum_i[\rho_i\ln\rho_i + (1-\rho_i)\ln(1-\rho_i)] \quad (1)$$

where $\rho_i$, the normalized density of fluid on site $i$, can continuously vary from 0 to 1, $\eta_i = 0$ or $\eta_i = 1$, indicating if site $i$ is occupied by solid or not. $w_{ff}$ and $w_{sf}$ are the fluid−fluid interactions and fluid−solid interactions, respectively, that are imported from atomistic simulation data.[37] The cement paste porous structure used here comes from the out-of-equilibrium precipitation of cohesive interactions of calcium silicate hydrate (C−S−H) nanograins and has a realistic pore size distribution (gel pores and capillary pores below and above 3 nm, respectively) and connectivity[35] (see the Supporting Information). They have volume fraction of 0.52 that corresponds to cement paste made with water to cement ratio (w/c) of 0.45.[47] The lattice spacing, $a$, of our DFT simulation is estimated from the surface tension that is energy per area $\gamma \approx w_{ff}/2a^2$ for nitrogen at $T = 77$ K, $\gamma \approx 8.94$ mN/m, which gives $a \approx 0.345$ nm; for water at $T = 300$ K, $\gamma \approx 72$ mN/m, which gives $a \approx 0.24$ nm. On the basis of these estimates, we choose a fine-grid cell size of $a = 0.3$ nm that is close to the molecular size. The fluid−fluid interaction, $w_{ff}$, is determined by the bulk critical point $k_BT_c = -\nu w_{ff}/2$, where $\nu$ ($\nu = 6$) is the number of nearest neighbors on the cubic lattice. The fluid−solid interaction, $w_{sf} = 2.5w_{ff}$, is estimated from molecular simulations of the isosteric heat of adsorption in the limit of zero coverage for water in the cement paste.[37]

Adopting the relation between chemical potential and relative saturating pressure, $h$ (or relative humidity in the case of water) $\mu = k_BT\ln(h)$, we show in Figure 1a that the lattice DFT method with appropriate grid fineness is able to quantitatively predict the room temperature hysteretic water adsorption/desorption isotherm in the cement paste in agreement with experiments[6,33,48,49] with no adjustable parameter. In particular, the closure point of the hysteresis loop ($h \approx 30\%$) in the simulated isotherms is one that is observed in many water adsorption experiments at room temperature in disordered mesoporous materials.[50]

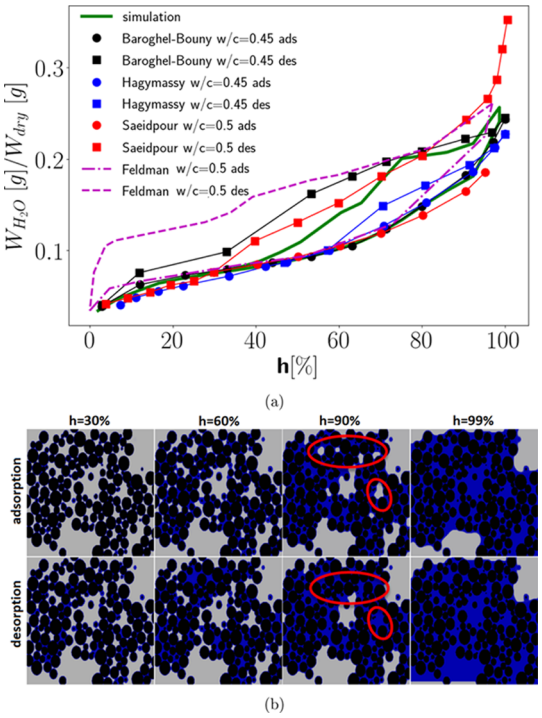


**Figure 1.** (a) Simulated water adsorption/desorption isotherm of a mesoscale cement paste model of volume fraction, $\eta = 0.52$[35] compared to experimental data.[6,33,48,49] The isotherm is renormalized with respect to the closure point. (b) Cross-section of the pore network showing water upon adsorption/desorption. Black—colloidal nanoparticles of CSH. Blue—water. Grey—vapor. Ink-bottleneck effect is exemplified by the red-circled areas.

There are many studies on water sorption in hardened cement paste reporting low pressure hysteresis loops in the adsorption/desorption isotherm.[39,49] This feature has been attributed to the exchange of water molecules from the interlayer void inside the cement hydrates nanograins and gel pores[51] similar to what is happening in clay that also exhibits low pressure hysteresis.[52−54] Specifically, calcium clay exhibits smaller residual swelling than sodium clay because of stronger ion−ion correlation forces (ICFs).[55] Calcium hydrate layers inside the nanograins are 4−5 times more charged than those in clay montmorillonite.[56] This corresponds to very large attractive electrostatic ICFs that probably do not allow swelling by contrast to clay. There is a long standing debate in literature that started 60 years ago with the seminal works of Feldman[39] and Hagymassy et al.[48] showing opposite conclusions on the existence of the low pressure water adsorption/desorption isotherm at room temperature. More recently, Saeidpour and Wadsö[33] using dynamic vapor sorption have shown the presence of a low pressure hysteresis. Along the same line, Baroghel-Bouny showed that water adsorption/desorption at 44 °C does not exhibit low pressure hysteresis, indicating that this is likely a kinetic issue due to deficient equilibrium conditions.[49] In this work, we are focusing only on the high pressure capillary effect, ($h > 30\%$) and its poromechanical consequences and, therefore, not considering the water exchange between the inside of cement hydrates nanograins and gel or capillary pores that is said to occur at relative humidity lower than 30%. We assume no volume change of the cement hydrates nanograins.[33,57]

The reversible part of the simulated adsorption/desorption isotherm curve shown in Figure 1a corresponds to the buildup of molecular nanometric films of various thicknesses depending on the local surface curvature. We found that metastable ink-bottleneck (cavitation) states[44] are at the origin of sorption hysteresis in cement paste as shown in Figure 1b. The high connectivity of the cement paste pore network and the resulting percolating liquid distribution is


DOI: 10.1021/acs.langmuir.8b03400
Langmuir 2019, 35, 4397−4402

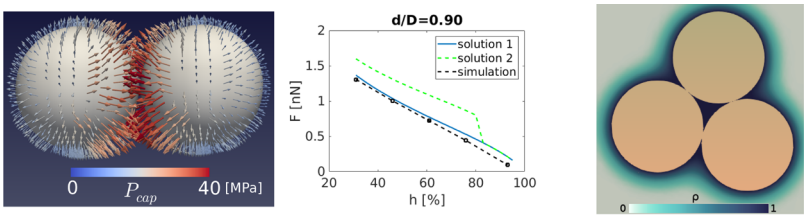


**Figure 2.** Capillary stress—(a) simulation of local stresses in the capillary bridge between two spherical colloidal particles of diameter $D$ = 6 nm at $h$ = 30%. (b) Total capillary force, $F$, on each particle (positive sign for pointing toward the other particle) vs humidity, $h$, compared with the two analytical solutions of the Kelvin−Laplace equation (because of the 3D geometry, see the Supporting Information eq 13) for sphere-center separation, $d = 0.9D$ (spherical particle diameter $D$ = 6 nm), including the surface adsorbed layer. (c) Cross-sectional view of the liquid density, $\rho$, filling the region between the three touching spherical particles, simulated at $h$ = 35%.

naturally obtained in our numerical framework without any ad hoc assumption on water distribution in contrast to the aforementioned pendular/funicular ring models.

**Capillary stress.** Next, we analyze the fluid distribution in the pore network (Figure 1b), and calculate the mechanical effect of capillary stress in such a complex porous structure. To calculate the capillary stress at a given $\mu$ (or $h$) value, the mean-field lattice gas DFT[36] is written in its continuum limit, which is equivalent to the Cahn−Hilliard phase-field model (see e.g., eq 3.18 from Cahn and Hilliard[58] and eq 59 from Bazant[59])

$$\Omega = \int (k_B T[\rho \ln(\rho) + (1-\rho)\ln(1-\rho)] - \mu\rho)\mathrm{d}\nu + \int \left[\frac{w_{ff}}{2}a^2(\vec{\nabla}\rho)^2 - \frac{w_{ff}}{2}\nu\rho^2\right]\mathrm{d}\nu + \int\int_{\partial V} \mathrm{d}\vec{S}\cdot\left(w_{sf}\rho\vec{n} - \frac{w_{ff}}{2}a^2\rho\vec{\nabla}\rho\right) \quad (2)$$

where the order parameter, $0 < \rho < 1$, here is the normalized liquid density, $\partial V$ represents the liquid−solid boundary, and all symbols are as explained after eq 1.

Once we have a suitable free energy, we define the capillary stress tensor, first derived by Korteweg[60,61] (see eq 4 from Anderson et al.[61])

$$\vec{\sigma} = \left(p_0(\rho) - \frac{a^2 w_{ff}}{2}(\vec{\nabla}\rho)^2\right)\vec{\mathbf{I}} + a^2 w_{ff}\rho\vec{\nabla}\otimes\rho\vec{\nabla} + \vec{\sigma}_0 \quad (3)$$

and use it to express the stress in terms of only the density profile from the DFT simulations in the porous structure. Here, $\vec{\mathbf{I}}$ is the identity tensor, $\vec{\sigma}_0$ is an arbitrary tensor constant, $p_0(\rho) = \mu\rho + \frac{\nu w_{ff}}{2}\rho^2 - k_B T[\rho\ln(\rho) + (1-\rho)\ln(1-\rho)]$ is the asymptotic bulk value of the hydrostatic pressure, and other symbols are the same as in eq 2 (see derivation for eq 3 in the Supporting Information). In principle, surface forces can be calculated by integrating the normal stress over the solid pore walls, but we find that this procedure leads to large errors for complex geometries.

We thus introduce the second step of our method, which uses Stokes' theorem[62] to deform the contour away from the solid surface and integrate the normal stress over a space-filling tessellation of the microstructure. In this way, equal and opposite forces are applied at each face of the tessellation, perfectly satisfying Newton's third law in the fluid, despite adsorbed fluid density fluctuations on the complex surface geometry. For colloidal or granular systems of convex particles, the most natural choice is the Voronoi tessellation, for which fast algorithms are available, such as the package Voro++[63] used below.

Using the lattice-gas DFT model for water, we first apply the method to the simplest case of two nanograins at short distance. Figure 2a shows a stable capillary bridge at appropriate relative humidity. Analytical results are available to describe the capillary force,[21,27,64] and most models for wet granular materials rely on this picture of a capillary bridge.[65−70] The simulated capillary force versus humidity is shown in Figure 2b, in agreement with the solution of the Kelvin−Laplace equation,[71−73] assuming bulk water surface tension. The forces are simulated on the adsorption branch and thus compared with the analytical solution that has the smaller Kelvin radius (in general the Kelvin equation for a capillary bridge between two spheres admits two solutions, see the Supporting Information), augmented by a wetting layer of thickness 0.25 nm.

Figure 2c shows three spheres nearly in contact to illustrate the challenges posed by any other geometry. At low humidity, the capillary bridge theory still holds and accurately predicts simulation results. However, at high humidity, these bridges coalesce to fill the region between the particles and drastically alter the forces, in a way that only a molecular-based approach can capture such as the DFT simulation used here. This is due in part to the liquid−vapor interface that takes a nonconvex shape in three dimensions.

Figure 3 shows the Voronoi tessellation[63] on the 3D heterogeneous porous packing of polydisperse cement nanograins[35] from which

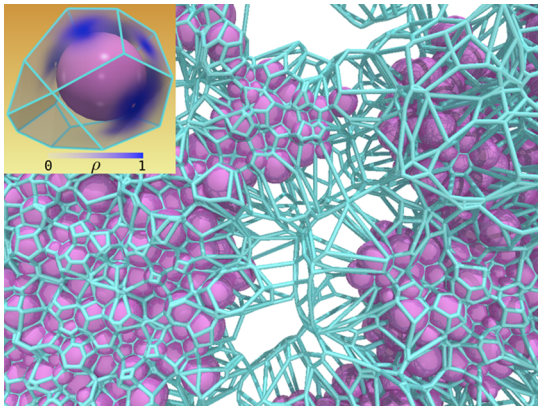


**Figure 3.** Slice of a polydisperse heterogeneous sphere packing, showing the Voronoi tessellation used to calculate capillary stresses, in the colloidal cement paste.[35] The inset shows adsorbed fluid density profile (blue) on the faces of the Voronoi cell for a single grain at $h$ = 30%.

stresses can be efficiently and accurately computed. This example demonstrates the capability to predict the stress and deformation of porous materials for any spatial distribution of confined fluid as in the case of equilibrium capillary condensation during drying and wetting processes or in out-of-equilibrium multiphase flow.

## RESULTS

Applying the capillary force on each nanograin in structural relaxation MD simulations, we compute the drying shrinkage of cement paste in quantitative agreement with the experimentally observed volume shrinkage (see Figure 4). Our findings indicate that capillary forces facilitate macro-



DOI: 10.1021/acs.langmuir.8b03400
Langmuir 2019, 35, 4397−4402

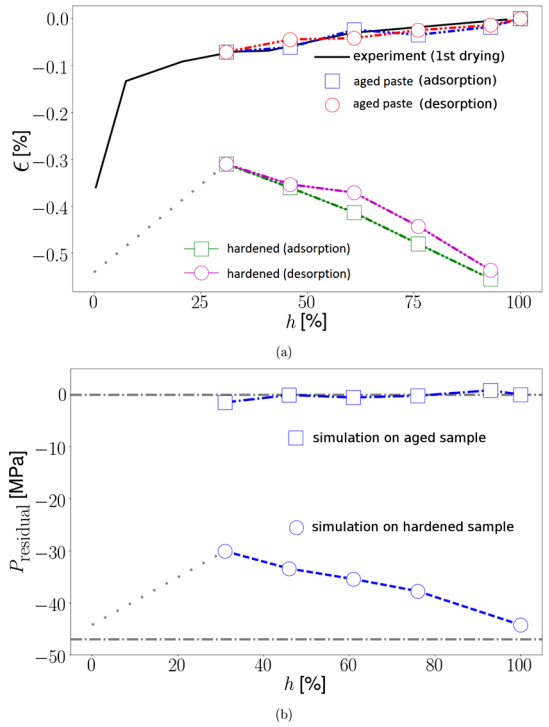


**Figure 4.** Stress relaxation of "hardened" and "aged" cement paste configurations in (a) constant pressure (*NPT*) and (b) constant volume (*NVT*) MD simulations under the action of capillary forces. The experimental data are from refs 39 and 51 for cement paste of w/c = 0.5.

scopic stress relaxation in granular or colloidal cohesive media with rough and glassy potential energy landscapes and having an abundance of metastable states.

Reactive heterogeneous materials such as cement contain residual stresses due to the out-of-equilibrium solidification process.[74−76] The cement paste structure analyzed here has accumulated tensile eigenstresses of −47 MPa because of the out-of-equilibrium precipitation of nanograins.[47,77] We refer to this structure as "hardened" cement paste. Then, the eigenstress was relaxed (less than 10 kPa) using energy minimization under *NPT* conditions (see the Supporting Information). The relaxed cement paste structure is named "aged".

Figure 4a shows how capillary forces influence the shrinkage strain of "hardened" and "aged" cement paste. In a series of MD structural relaxation simulations, capillary forces calculated at corresponding relative humidities, *h*, were applied on the nanograins as force vectors in addition to the cohesive interactions of cement hydrates nanograins (see the Supporting Information). The "aged" model exhibits shrinkage only because of the capillary effect, whereas the "hardened" sample shrinks under the combined action of tensile eigenstresses and capillary forces. In the "aged" sample, the pure capillary effect decreases with increasing humidity, and the predicted strain is in agreement with the experiment[39] for $h > 30\%$ on the first drying cycle. In contrast, the "hardened" sample shrinks more than the "aged" one and with the opposite trend: the amount of shrinkage strain increases upon increasing humidity. This counter-intuitive behavior was also observed in short-term cycling *h* cement experiments after long-term curing of the cement paste samples under a series of constant relative humidities.[42] Our relaxation scheme with capillary forces at constant *h* coupled to nanograins cohesive interactions would correspond to the long-term curing conditions of the experiments in ref 42. It is interesting to note that our relative strain results are in surprisingly good agreement with the total strain measurement of Figure 4 in ref 42.

In Figure 4b, we investigated stress relaxation under constant volume constraint. Minimal residual stresses are observed in the "aged" paste for all humidities. Residual stresses in the "hardened" paste were relaxed to −30 MPa at $h = 30\%$ (closure point of the hysteresis loop), which is significantly different than that obtained under dry condition (−44 MPa). Overall, capillary forces help in relaxing eigenstresses with the lowest volume shrinkage. It is remarkable to notice the synergistic effect of capillaries and eigenstresses, reducing the shrinkage compared to dry or fully saturated conditions.

These results demonstrate that capillary stress at intermediate humidity is an effective mechanism of eigenstress relaxation that is developed during setting and, therefore, beneficial to cement durability. Although the magnitude of capillary forces on each nanograin is small (∼1 nN) compared to the grain−grain interactions (∼10 nN), these forces still have an observable effect at the mesoscale. For materials that are "softer" than cement paste (e.g., wood,[78] biopolymers[79]), capillary forces are expected to have even larger aging effects.

## CONCLUSIONS

In conclusion, we have demonstrated that a mean-field lattice DFT approach with suitable molecular scale energy parameters and lattice discretization fineness is able to predict the hysteretic adsorption/desorption isotherm of water in a realistic mesoscale cement paste model, further validating this colloidal description of cement hydrates. We further extended this DFT approach to calculate capillary stress from the confined fluid distribution and formulated a general framework to calculate capillary stress in complex porous media, without any assumptions on the pore morphology or topology, across the full range of liquid saturation. Interestingly enough, we found that when combined with the cohesive interactions of the nanograins, the capillary stress at *h* 30% actually helps in removing the eigenstress of the cement paste that results from the out-of-equilibrium setting conditions. Our approach is to predict for the first time capillary stress and structural relaxation in cement paste based on statistical physics combined with a realistic mesoscale texture, taking into account fluid−solid coupling explicitly. This is of both theoretical and practical importance because of cement's multiscale challenging texture and its wide usage in everyday life.

## ASSOCIATED CONTENT

### Supporting Information

The Supporting Information is available free of charge on the ACS Publications website at DOI: 10.1021/acs.langmuir.8b03400.

Phase-field formulation and capillary stress calculation, numerical simulations, microstructure of cement paste, simulation of adsorption/desorption isotherms, and structural relaxation with capillary stress. (PDF)



DOI: 10.1021/acs.langmuir.8b03400
*Langmuir* 2019, 35, 4397−4402

## AUTHOR INFORMATION


### Corresponding Authors

*E-mail: pellenq@mit.edu (R.J.-M.P.).
*E-mail: bazant@mit.edu (M.Z.B.).

### ORCID

Enrico Masoero: 0000-0003-1791-6640
Mohammad Mirzadeh: 0000-0003-2781-1033
Roland J.-M. Pellenq: 0000-0001-5559-4190


### Notes

The authors declare no competing financial interest.

## ACKNOWLEDGMENTS

This work was supported by the Concrete Sustainability Hub at MIT, CNRS and the A*MIDEX foundation. The authors thank F.-J. Ulm, S. Yip, N. Nadkarni, and S. Moeini for useful discussions and C. Rycroft for help with visualization.

## REFERENCES


(1) Bocquet, L.; Charlaix, E.; Ciliberto, S.; Crassous, J. Moisture-induced ageing in granular media and the kinetics of capillary condensation. *Nature* **1998**, *396*, 735−737.
(2) Li, K. W.; Hsu, Y.-W.; Chang, W.-R.; Lin, C.-H. Friction measurements on three commonly used floors on a college campus under dry, wet, and sand-covered conditions. *Saf. Sci.* **2007**, *45*, 980−992.
(3) Binggeli, M.; Mate, C. M. Influence of capillary condensation of water on nanotribology studied by force microscopy. *Appl. Phys. Lett.* **1994**, *65*, 415−417.
(4) Burdine, N. T. Relative permeability calculations from pore size distribution data. *J. Petrol. Technol.* **1953**, *5*, 71−78.
(5) Corey, A. T. The interrelation between gas and oil relative permeabilities. *Prod. Mon.* **1954**, *19*, 38−41.
(6) Feldman, R. F.; Sereda, P. J. A model for hydrated Portland cement paste as deduced from sorption-length change and mechanical properties. *Mater. Struct.* **1968**, *1*, 509−520.
(7) Igarashi, S.-i.; Bentur, A.; Kovler, K. Autogenous shrinkage and induced restraining stresses in high-strength concretes. *Cem. Concr. Res.* **2000**, *30*, 1701−1707.
(8) Coussy, O. *Mechanics and Physics of Porous Solids*; John Wiley & Sons, 2011.
(9) Singh, K. B.; Tirumkudulu, M. S. Cracking in drying colloidal films. *Phys. Rev. Lett.* **2007**, *98*, 218302.
(10) Routh, A. F. Drying of thin colloidal films. *Rep. Prog. Phys.* **2013**, *76*, 046603.
(11) Tirumkudulu, M. S.; Russel, W. B. Cracking in drying latex films. *Langmuir* **2005**, *21*, 4938−4948.
(12) Suh, K. Y.; Lee, H. H. Capillary Force Lithography: Large-Area Patterning, Self-Organization, and Anisotropic Dewetting. *Adv. Funct. Mater.* **2002**, *12*, 405−413.
(13) Hor, J. L.; Jiang, Y.; Ring, D. J.; Riggleman, R. A.; Turner, K. T.; Lee, D. Nanoporous Polymer-Infiltrated Nanoparticle Films with Uniform or Graded Porosity via Undersaturated Capillary Rise Infiltration. *ACS Nano* **2017**, *11*, 3229−3236.
(14) Manohar, N.; Stebe, K. J.; Lee, D. Solvent-Driven Infiltration of Polymer (SIP) into Nanoparticle Packings. *ACS Macro Lett.* **2017**, *6*, 1104−1108.
(15) Manoharan, V. N.; Elsesser, M. T.; Pine, D. J. Dense packing and symmetry in small clusters of microspheres. *Science* **2003**, *301*, 483−487.
(16) Schnall-Levin, M.; Lauga, E.; Brenner, M. P. Self-assembly of spherical particles on an evaporating sessile droplet. *Langmuir* **2006**, *22*, 4547−4551.
(17) Lauga, E.; Brenner, M. P. Evaporation-driven assembly of colloidal particles. *Phys. Rev. Lett.* **2004**, *93*, 238301.
(18) Cho, Y.-S.; Yi, G.-R.; Lim, J.-M.; Kim, S.-H.; Manoharan, V. N.; Pine, D. J.; Yang, S.-M. Self-organization of bidisperse colloids in water droplets. *J. Am. Chem. Soc.* **2005**, *127*, 15968−15975.
(19) Larson, N. M.; Zok, F. W. Insights from in-situ X-ray computed tomography during axial impregnation of unidirectional fiber beds. *Composites, Part A* **2018**, *107*, 124−134.
(20) Fanale, F. P.; Cannon, W. A. Mars: CO2 adsorption and capillary condensation on clays-significance for volatile storage and atmospheric history. *J. Geophys. Res.: Solid Earth* **1979**, *84*, 8404−8414.
(21) Scholtès, L.; Hicher, P.-Y.; Nicot, F.; Chareyre, B.; Darve, F. On the capillary stress tensor in wet granular materials. *Int. J. Numer. Anal. Methods Geomech.* **2009**, *33*, 1289−1313.
(22) Wang, K.; Sun, W. Anisotropy of a tensorial Bishop's coefficient for wetted granular materials. *J. Eng. Mech.* **2017**, *143*, B4015004.
(23) Duriez, J.; Wan, R. Stress in wet granular media with interfaces via homogenization and discrete element approaches. *J. Eng. Mech.* **2016**, *142*, 04016099.
(24) Ravikovitch, P. I.; Neimark, A. V. Density functional theory model of adsorption deformation. *Langmuir* **2006**, *22*, 10864−10868.
(25) Jakubov, T. S.; Mainwaring, D. E. Adsorption-induced dimensional changes of solids. *Phys. Chem. Chem. Phys.* **2002**, *4*, 5678−5682.
(26) Gor, G. Y.; Neimark, A. V. Adsorption-induced deformation of mesoporous solids. *Langmuir* **2010**, *26*, 13021−13027.
(27) Andrienko, D.; Patrício, P.; Vinogradova, O. I. Capillary bridging and long-range attractive forces in a mean-field approach. *J. Chem. Phys.* **2004**, *121*, 4414−4423.
(28) Melnikov, K.; Wittel, F. K.; Herrmann, H. J. Micro-mechanical failure analysis of wet granular matter. *Acta Geotech.* **2016**, *11*, 539−548.
(29) Melnikov, K.; Mani, R.; Wittel, F. K.; Thielmann, M.; Herrmann, H. J. Grain-scale modeling of arbitrary fluid saturation in random packings. *Phys. Rev. E: Stat., Nonlinear, Soft Matter Phys.* **2015**, *92*, 022206.
(30) Gor, G. Y.; Huber, P.; Bernstein, N. Adsorption-induced deformation of nanoporous materials−A review. *Appl. Phys. Rev.* **2017**, *4*, 011303.
(31) Schappert, K.; Pelster, R. Unexpected sorption-induced deformation of nanoporous glass: Evidence for spatial rearrangement of adsorbed argon. *Langmuir* **2014**, *30*, 14004−14013.
(32) Eriksson, J. C. Thermodynamics of surface phase systems: V. Contribution to the thermodynamics of the solid-gas interface. *Surf. Sci.* **1969**, *14*, 221−246.
(33) Saeidpour, M.; Wadsö, L. Moisture equilibrium of cement based materials containing slag or silica fume and exposed to repeated sorption cycles. *Cem. Concr. Res.* **2015**, *69*, 88−95.
(34) Silvestre-Albero, A. M.; Juárez-Galán, J. M.; Silvestre-Albero, J.; Rodríguez-Reinoso, F. Low-pressure hysteresis in adsorption: an artifact? *J. Phys. Chem. C* **2012**, *116*, 16652−16655.
(35) Ioannidou, K.; Krakowiak, K. J.; Bauchy, M.; Hoover, C. G.; Masoero, E.; Yip, S.; Ulm, F.-J.; Levitz, P.; Pellenq, R. J.-M.; Del Gado, E. Mesoscale texture of cement hydrates. *Proc. Natl. Acad. Sci. U.S.A.* **2016**, *113*, 2029−2034.
(36) Kierlik, E.; Monson, P. A.; Rosinberg, M. L.; Tarjus, G. Adsorption hysteresis and capillary condensation in disordered porous solids: a density functional study. *J. Phys.: Condens. Matter* **2002**, *14*, 9295.
(37) Bonnaud, P. A.; Ji, Q.; Coasne, B.; Pellenq, R. J.-M.; Van Vliet, K. J. Thermodynamics of water confined in porous calcium-silicate-hydrates. *Langmuir* **2012**, *28*, 11422−11432.
(38) Pellenq, R. J.-M.; Levitz, P. E. Capillary condensation in a disordered mesoporous medium: a grand canonical Monte Carlo study. *Mol. Phys.* **2002**, *100*, 2059−2077.
(39) Feldman, R. Sorption and Length Change, Scanning Isotherms of Methanol and Water on Hydrated Portland Cement. *Proceedings of the Fifth International Symposium on the Chemistry of Cement*: Tokyo, 1968.




DOI: 10.1021/acs.langmuir.8b03400
*Langmuir* 2019, 35, 4397−4402

(40) Parrott, L. J. The effect of moisture content upon the elasticity of hardened cement paste. *Mag. Concr. Res.* **1973**, *25*, 17−20.
(41) Scherer, G. W. Drying, shrinkage, and cracking of cementitious materials. *Transp. Porous Media* **2015**, *110*, 311−331.
(42) Maruyama, I.; Igarashi, G.; Nishioka, Y. Bimodal behavior of CSH interpreted from short-term length change and water vapor sorption isotherms of hardened cement paste. *Cem. Concr. Res.* **2015**, *73*, 158−168.
(43) Kierlik, E.; Monson, P.; Rosinberg, M.; Sarkisov, L.; Tarjus, G. Capillary condensation in disordered porous materials: Hysteresis versus equilibrium behavior. *Phys. Rev. Lett.* **2001**, *87*, 055701.
(44) Coasne, B.; Galarneau, A.; Pellenq, R. J. M.; Di Renzo, F. Adsorption, intrusion and freezing in porous silica: the view from the nanoscale. *Chem. Soc. Rev.* **2013**, *42*, 4141−4171.
(45) Detcheverry, F.; Kierlik, E.; Rosinberg, M. L.; Tarjus, G. Mechanisms for gas adsorption and desorption in silica aerogels: The effect of temperature. *Langmuir* **2004**, *20*, 8006−8014.
(46) Kierlik, E.; Rosinberg, M. L.; Tarjus, G.; Viot, P. Equilibrium and out-of-equilibrium (hysteretic) behavior of fluids in disordered porous materials: Theoretical predictions. *Phys. Chem. Chem. Phys.* **2001**, *3*, 1201−1206.
(47) Ioannidou, K.; Del Gado, E.; Ulm, F.-J.; Pellenq, R. J.-M. Inhomogeneity in Cement Hydrates: Linking Local Packing to Local Pressure. *J. Nanomech. Micromech.* **2017**, *7*, 04017003.
(48) Hagymassy, J.; Odler, I.; Yudenfreund, M.; Skalny, J.; Brunauer, S. Pore structure analysis by water vapor adsorption. III. Analysis of hydrated calcium silicates and portland cements. *J. Colloid Interface Sci.* **1972**, *38*, 20−34.
(49) Baroghel-Bouny, V. Water vapour sorption experiments on hardened cementitious materials: Part I: Essential tool for analysis of hygral behaviour and its relation to pore structure. *Cem. Concr. Res.* **2007**, *37*, 414−437.
(50) Naono, H.; Hakuman, M. Analysis of porous texture by means of water vapor adsorption isotherm with particular attention to lower limit of hysteresis loop. *J. Colloid Interface Sci.* **1993**, *158*, 19−26.
(51) Pinson, M. B.; Masoero, E.; Bonnaud, P. A.; Manzano, H.; Ji, Q.; Yip, S.; Thomas, J. J.; Bazant, M. Z.; Van Vliet, K. J.; Jennings, H. M. Hysteresis from multiscale porosity: Modeling water sorption and shrinkage in cement paste. *Phys. Rev. Appl.* **2015**, *3*, 064009.
(52) Cases, J. M.; Bérend, I.; François, M.; Uriot, J.; Michot, L.; Thomas, F. Mechanism of adsorption and desorption of water vapor by homoionic montmorillonite; 3, The Mg2+, Ca2+, and Ba3+ exchanged forms. *Clays Clay Miner.* **1997**, *45*, 8−22.
(53) Michot, L. J.; Bihannic, I.; Pelletier, M.; Rinnert, E.; Robert, J.-L. Hydration and swelling of synthetic Na-saponites: Influence of layer charge. *Am. Mineral.* **2005**, *90*, 166−172.
(54) Tambach, T. J.; Bolhuis, P. G.; Hensen, E. J. M.; Smit, B. Hysteresis in clay swelling induced by hydrogen bonding: accurate prediction of swelling states. *Langmuir* **2006**, *22*, 1223−1234.
(55) Segad, M.; Jönsson, B.; Åkesson, T.; Cabane, B. Ca/Na montmorillonite: structure, forces and swelling properties. *Langmuir* **2010**, *26*, 5782−5790.
(56) Pellenq, R. J.-M.; Caillol, J. M.; Delville, A. Electrostatic Attraction between Two Charged Surfaces: A (N,V,T) Monte Carlo Simulation. *J. Phys. Chem. B* **1997**, *101*, 8584−8594.
(57) Wu, M.; Johannesson, B.; Geiker, M. A study of the water vapor sorption isotherms of hardened cement pastes: Possible pore structure changes at low relative humidity and the impact of temperature on isotherms. *Cem. Concr. Res.* **2014**, *56*, 97−105.
(58) Cahn, J. W.; Hilliard, J. E. Free energy of a nonuniform system. I. Interfacial free energy. *J. Chem. Phys.* **1958**, *28*, 258−267.
(59) Bazant, M. Z. Theory of chemical kinetics and charge transfer based on nonequilibrium thermodynamics. *Acc. Chem. Res.* **2013**, *46*, 1144−1160.
(60) Korteweg, D. J. Sur la forme que prennent les équations du mouvements des fluides si l'on tient compte des forces capillaires causées par des variations de densité considérables mais connues et sur la théorie de la capillarité dans l'hypothèse d'une variation continue de la densité. *Archives Néerlandaises des Sciences exactes et naturelles* **1901**, *6*, 1−24.
(61) Anderson, D. M.; McFadden, G. B.; Wheeler, A. A. Diffuse-interface methods in fluid mechanics. *Annu. Rev. Fluid. Mech.* **1998**, *30*, 139−165.
(62) Landau, L.; Lifšic, E.; Sykes, J.; Reid, W. *Course of Theoretical Physics; Teoretičeskaja fizika*; Butterworth-Heinenann, 1987.
(63) Rycroft, C. *Voro++: A Three-Dimensional Voronoi Cell Library in C++*, 2009,
(64) Cheng, T.-L.; Wang, Y. U. Spontaneous formation of stable capillary bridges for firming compact colloidal microstructures in phase separating liquids: a computational study. *Langmuir* **2012**, *28*, 2696−2703.
(65) Kohonen, M. M.; Geromichalos, D.; Scheel, M.; Schier, C.; Herminghaus, S. On capillary bridges in wet granular materials. *Phys. A* **2004**, *339*, 7−15.
(66) Scheel, M.; Seemann, R.; Brinkmann, M.; Di Michiel, M.; Sheppard, A.; Herminghaus, S. Liquid distribution and cohesion in wet granular assemblies beyond the capillary bridge regime. *J. Phys.: Condens. Matter* **2008**, *20*, 494236.
(67) Mitarai, N.; Nori, F. Wet granular materials. *Adv. Phys.* **2006**, *55*, 1−45.
(68) Richefeu, V.; El Youssoufi, M. S.; Radjai, F. Shear strength properties of wet granular materials. *Phys. Rev. E: Stat., Nonlinear, Soft Matter Phys.* **2006**, *73*, 051304.
(69) Herminghaus, S. Dynamics of wet granular matter. *Adv. Phys.* **2005**, *54*, 221−261.
(70) Fournier, Z.; Geromichalos, D.; Herminghaus, S.; Kohonen, M. M.; Mugele, F.; Scheel, M.; Schulz, M.; Schulz, B.; Schier, C.; Seemann, R.; Skudelny, A. Mechanical properties of wet granular materials. *J. Phys.: Condens. Matter* **2005**, *17*, S477.
(71) Barrett, E. P.; Joyner, L. G.; Halenda, P. P. The determination of pore volume and area distributions in porous substances. I. Computations from nitrogen isotherms. *J. Am. Chem. Soc.* **1951**, *73*, 373−380.
(72) Thomson, W. On the equilibrium of vapour at a curved surface of liquid. *Proc. R. Soc. Edinburgh* **1872**, *7*, 63−68.
(73) Stifter, T.; Marti, O.; Bhushan, B. Theoretical investigation of the distance dependence of capillary and van der Waals forces in scanning force microscopy. *Phys. Rev. B: Condens. Matter Mater. Phys.* **2000**, *62*, 13667.
(74) Abuhaikal, M. M. A. Expansion and shrinkage of early age cementitious materials under saturated conditions: the role of colloidal eigenstresses. Ph.D. Thesis, Massachusetts Institute of Technology, 2016.
(75) Ulm, F.-J.; Pellenq, R. J. M. Shrinkage Due to Colloidal Force Interactions. *Proceedings of the CONCREEP10 Conference, Vienna, Austria, Sept 2015*; Hellmich, C., Ed.; ASCE Pub, 2015; Vol. *13*−*16*.
(76) Abuhaikal, M.; Ioannidou, K.; Petersen, T.; Pellenq, R. J.-M.; Ulm, F.-J. Le Châtelier's conjecture: Measurement of colloidal eigenstresses in chemically reactive materials. *J. Mech. Phys. Solids* **2018**, *112*, 334−344.
(77) Ioannidou, K.; Pellenq, R. J.-M.; Del Gado, E. Controlling local packing and growth in calcium−silicate−hydrate gels. *Soft Matter* **2014**, *10*, 1121−1133.
(78) Patera, A.; Derome, D.; Griffa, M.; Carmeliet, J. Hysteresis in swelling and in sorption of wood tissue. *J. Struct. Biol.* **2013**, *182*, 226−234.
(79) Kulasinski, K.; Guyer, R.; Keten, S.; Derome, D.; Carmeliet, J. Impact of moisture adsorption on structure and physical properties of amorphous biopolymers. *Macromolecules* **2015**, *48*, 2793−2800.



DOI: 10.1021/acs.langmuir.8b03400
*Langmuir* 2019, 35, 4397−4402